sensors

MDPI

Article

Fabrication Technology and Characteristics Research of a Monolithically-Integrated 2D Magnetic Field Sensor Based on Silicon Magnetic Sensitive Transistors

Xiaofeng Zhao *, Chenchen Jin, Qi Deng, Meiwei Lv and Dianzhong Wen

School of Electronics Engineering, Heilongjiang University, Harbin 150080, China; 2161330@s.hlju.edu.cn (C.J.); 2151254@s.hlju.edu.cn (Q.D.); 2171251@s.hlju.edu.cn (M.L.); wendianzhong@hlju.edu.cn (D.W.)

* Correspondence: zhaoxiaofeng@hlju.edu.cn; Tel.: +86-451-8660-8457

Received: 9 June 2018; Accepted: 26 July 2018; Published: 4 August 2018

Abstract: A monolithically-integrated two-dimensional (2D) magnetic field sensor consisting of two difference structures (DSI and DSII) is proposed in this paper. The DSI and DSII are composed of four silicon magnetic sensitive transistors (SMST1, SMST2, SMST3 and SMST4) and four collector load resistors (R_{L1}, R_{L2}, R_{L3} and R_{L4}). Based on the magnetic sensitive principle of SMST, the integrated difference structure can detect magnetic fields' component (B_x and B_y) along the x-axis and y-axis, respectively. By adopting micro-electromechanical systems (MEMS) and packaging technology, the chips were fabricated on a p-type <100> orientation silicon wafer with high resistivity and were packaged on printed circuit boards (PCBs). At room temperature, when the V_{CE} = 5.0 V and I_B = 8.0 mA, the magnetic sensitivities (S_{xx} and S_{yy}) along the x-axis and the y-axis were 223 mV/T and 218 mV/T, respectively. The results show that the proposed sensor can not only detect the 2D magnetic field vector ($\boldsymbol{B}$) in the xy plane, but also that S_{xx} and S_{yy} exhibit good uniformity.

Keywords: two-dimensional magnetic field sensor; silicon magnetic sensitive transistor; monolithic integration; difference structure; MEMS technology

1. Introduction

At present, magnetic field sensors include the Hall element, giant magnetoresistance (GMR), tunneling magnetoresistance (TMR), magnetic sensitive diodes (MSD), silicon magnetic sensitive transistors (SMST), and so on [1–4]. With the development of microelectromechanical systems (MEMS) technology, magnetic field sensors have achieved a three-dimensional structure, miniaturization and integration and have a wide range of applications, such as industrial, military, aerospace and other areas [5–8]. In 2012, Chih-Ping Yu et al. proposed a two-dimensional difference folded Hall device, which integrated the lateral magnetic transistor (LMT) with the magnetoresistor (MR) [9]. When the bias current was 100 mA and the supply voltage was 2.7 V, the results show that the optimum magnetosensitivity (S_{RI}), optimum sensitivity (S), minimum nonlinearity error (NLE) and minimum offset were 0.385 V/(A·T), 9.564 mV/T, 4.03% and 18.85 mV, respectively. In 2013, Guo-Ming Sung et al. proposed a vertical Hall device (VHD) based on the combined magnetic effects between a bulk magnetotransistor (BMT), a vertical magnetoresistor (VMR) and a vertical magnetotransistor (VMT), which was sensitive to the magnetic induction in the plane [10]. The p-substrate was used to enhance the magnetosensitivity of BMT. The maximum supply-current-related magnetic sensitivity (S_I), maximum supply-voltage-related magnetic sensitivity (S_V) and minimum mean NLE were 1.92 V/(A·T), 42.65 mV/(V·T) and 2.11%, respectively. In 2015, Haiyun Huang et al. proposed a monolithic complementary metal oxide semiconductor (CMOS) magnetic Hall sensor with high

sensitivity and linearity characteristics [11]. The current-related sensitivity (S_I) and the voltage related sensitivity (S_V) achieved were 250 V/(A·T) at a 1-mA biasing current and 0.034 V/(V·T) at a bias voltage of 3 V. In 2017, a packaging integrated 2D magnetic field sensor was proposed, which consisted of four discrete SMSTs (the area of an SMST is 2.0 × 2.0 mm^2) and four load resistors [12]. When the V_{CE} = 10.0 V and I_B = 6.0 mA, the magnetic sensitivities of the sensor along the x-axis and y-axis were 366.0 mV/T and 365.0 mV/T, respectively. By combining or integrating multiple magnetic sensitive devices, the 2D magnetic field (B_x and B_y) in the xy plane can be measured. Based on the above references, the characteristics of sensitivity, uniformity and cross interference have been thoroughly studied. These properties have been improved by technological improvement and structural optimization. Summing up, monolithic integration has achieved greater improvement in uniformity and reduced cross interference.

In this paper, a monolithically-integrated 2D magnetic field sensor was designed and fabricated by MEMS technology. In order to improve the magnetic sensitivity and uniformity, we integrated two difference structures (DSI and DSII) with four SMSTs and four collector resistors as a magnetic sensitive structure along the direction of the x-axis and y-axis, respectively. On this basis, theoretical analysis shows the effect of the magnetic field component (B_x and B_y) on the output voltage of the proposed sensor. Meanwhile, the I_C-V_{CE} characteristics of SMSTs and the magnetic sensitivity of DSI and DSII were tested, and we studied the uniformity and cross interference of the magnetic sensitivity (S_{xx} and S_{yy}).

2. Basic Structure and Working Principle

2.1. Basics Structure

Figure 1 shows the cubic structure of the monolithically-integrated two-dimensional (2D) magnetic field sensor, which is made up of two difference structures. The DSI consists of two SMSTs (SMST1 and SMST2) and two collector load resistors (R_{L1} and R_{L2}) that can detect the magnetic field (B_x) along x-axis, and two SMSTs with the opposite magnetic sensitive direction are placed symmetrically along the x-axis in xy plane. The DSII is composed of two SMSTs (SMST3 and SMST4) and two collector load resistors (R_{L3} and R_{L4}) that exhibit the opposite magnetic sensitive direction along the y-axis. As shown in Figure 1a,b, four bases (B_1, B_2, B_3, B_4) and four collectors (C_1, C_2, C_3, C_4) are designed on the chip surface, and four emitters (E_1, E_2, E_3, E_4) are designed on the back of the chip by MEMS technology. Figure 1c,d shows the cross-section of the proposed sensor along the aa′ and bb′ directions, where L is the length of the base region, w is the width of the base region and $w > L_D$ (L_D is the carrier diffusion length), d is the thickness of the silicon membranes and θ is the angle between the external magnetic field vector ($\boldsymbol{B}$) and the $+x$-axis of the chip surface. As illustrated in Figure 1a, the external magnetic field along the $+x$-axis (or $+y$-axis) is defined as a positive magnetic field $B_x > 0$ T (or $B_y > 0$ T), and the opposite direction is defined as the reverse magnetic field $B_x < 0$ T (or $B_y < 0$ T).

2.2. Working Principle

Figure 2 presents an equivalent circuit of the proposed sensor, where the red dashed box consists of four SMSTs and four collector load resistors for the monolithically-integrated chip, in which R_{L1}, R_{L2}, R_{L3} and R_{L4} are the collector load resistors of four SMSTs, respectively. One end of R_{L1}, R_{L2}, R_{L3} and R_{L4} is connected to C_1, C_2, C_3 and C_4 of the SMSTs, respectively, and the other ends of R_{L1}, R_{L2}, R_{L3} and R_{L4} are connected to the supply power. V_{x1}, V_{x2}, V_{y3} and V_{y4} are the collector output voltages for SMST1, SMST2, SMST3 and SMST4, respectively. I_{B1}, I_{B2}, I_{B3} and I_{B4} are current sources that provide the base injection currents for B_1, B_2, B_3 and B_4, respectively. V_{DD} is the supply voltage. The four emitters of SMSTs are commonly grounded.

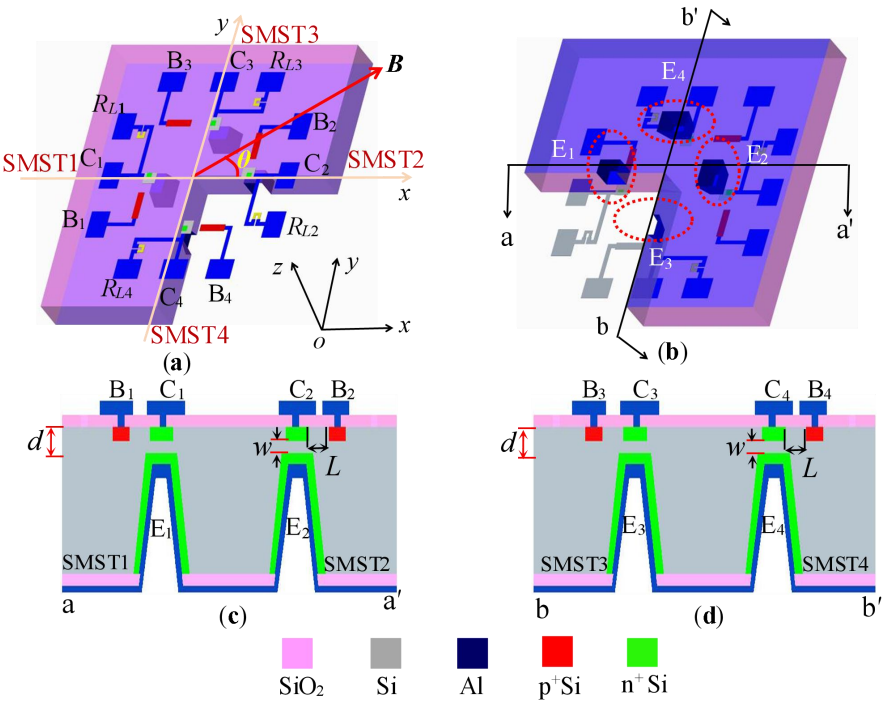

Figure 1. The basic structure of the monolithically-integrated 2D magnetic field sensor: (**a**) front of the basic structure; (**b**) back of the basic structure; (**c**) cross-section along aa′; (**d**) cross-section along bb′. SMST, silicon magnetic sensitive transistor.

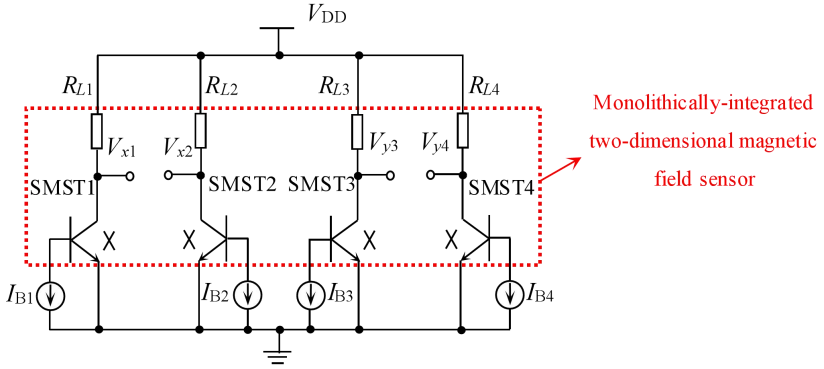

Figure 2. Equivalent circuit of the monolithically-integrated 2D magnetic field sensor.

As shown in Figure 3a, $\boldsymbol{B}$ is the magnetic field vector in the xy plane, where θ is the angle between $\boldsymbol{B}$ and the $+x$-axis. The magnetic field components B_x and B_y along the x-axis and the y-axis are expressed as:

$$\begin{cases} B_x = B\cos\theta \\ B_y = B\sin\theta \end{cases} \quad (1)$$

where B is magnetic induction intensity.

When B = 0 T, in ideal conditions, the carriers (electrons and holes) are not affected by the Lorentz force and are not deflected, so the collector currents of the four SMSTs are equal ($I_{C1} = I_{C2} = I_{C3} = I_{C4} = I_{C0}$).

As shown in Figure 3b, under the condition of $R_{L1} = R_{L2} = R_{L3} = R_{L4} = R_0$, the output voltages ($V_x$ and V_y) of the proposed sensor are as follows:

$$\begin{cases} V_x = V_{x1} - V_{x2} = I_{C2} \cdot R_{L2} - I_{C1} \cdot R_{L1} = 0 \\ V_y = V_{y3} - V_{y4} = I_{C4} \cdot R_{L4} - I_{C3} \cdot R_{L3} = 0 \end{cases} \tag{2}$$

where I_{C1}, I_{C2}, I_{C3} and I_{C4} are the collector currents of four SMSTs, respectively.

As shown in Figure 3c, when $B \neq 0$ T, under the action of B_x ($B_x > 0$), the carrier of SMST1 (SMST2) is deflected by the Lorentz force, leading to a decrease (increase) in the number of carriers collected by the collector region, so that I_{C1} decreases (I_{C2} increases). Similarly, under the action of B_y ($B_y > 0$), I_{C3} and I_{C4} of SMST3 and SMST4 are decreased and increased, respectively. V_x and V_y are expressed as:

$$\begin{cases} V_x = V_{x1} - V_{x2} = (I_{C1} + \Delta I_{C2}) \cdot R_{L2} - (I_{C1} + \Delta I_{C1}) \cdot R_{L1} = \Delta V_{x2} - \Delta V_{x1} \\ V_y = V_{y3} - V_{y4} = (I_{C4} + \Delta I_{C4}) \cdot R_{L4} - (I_{C3} + \Delta I_{C3}) \cdot R_{L3} = \Delta V_{y4} - \Delta V_{y3} \end{cases} \tag{3}$$

where ΔV_{x1}, ΔV_{x2}, ΔV_{y3} and ΔV_{y4} are the variations of the collector output voltages of SMST1, SMST2, SMST3 and SMST4, respectively. ΔI_{C1}, ΔI_{C2}, ΔI_{C3} and ΔI_{C4} are the variations of collector currents of four SMSTs, respectively.

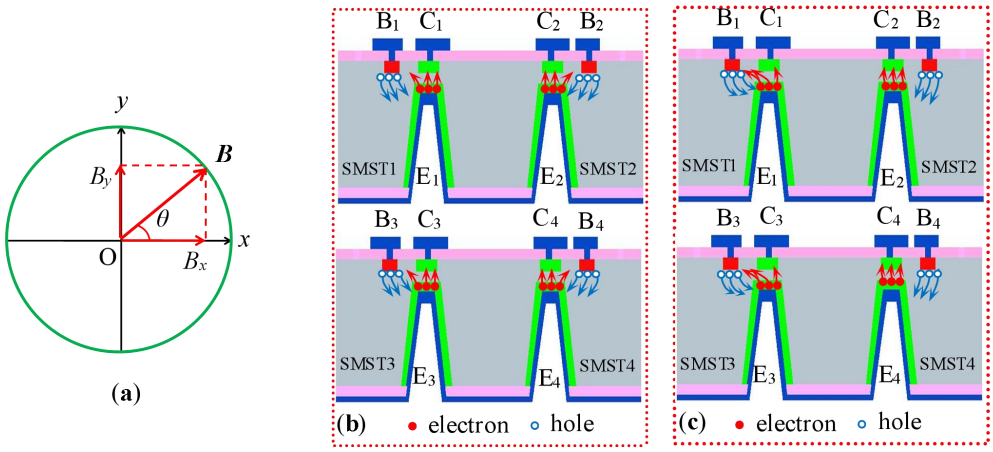

Figure 3. Working principle of the monolithically-integrated 2D magnetic field sensor: (**a**) magnetic field vector in the *xy* plane; (**b**) $B = 0$ T; (**c**) $B \neq 0$ T.

According to the definition of the magnetic sensitivities for the proposed sensor, the voltage magnetic sensitivities (S_{xx} and S_{yy}) along the *x*-axis and *y*-axis can be given:

$$\begin{cases} S_{xx} = \frac{|V_x|}{B_x} = \frac{|\Delta V_{x2} - \Delta V_{x1}|}{B_x} = |S_{x1} + S_{x2}| \\ S_{yy} = \frac{|V_y|}{B_y} = \frac{|\Delta V_{y4} - \Delta V_{y2}|}{B_y} = |S_{y3} + S_{y4}| \end{cases} \tag{4}$$

where S_{x1}, S_{x2}, S_{y3} and S_{y4} are the voltage magnetic sensitivities of SMST1, SMST2, SMST3 and SMST4, respectively.

Through theoretical analysis, magnetic field sensor with the difference structure of SMSTs can improve the magnetic sensitivity. On the basis of Equations (1)–(3), V_x and V_y can be obtained:

$$\begin{pmatrix} V_x \\ V_y \end{pmatrix} = \begin{pmatrix} S_{xx} & S_{xy} \\ S_{yx} & S_{yy} \end{pmatrix} \begin{pmatrix} B_x \\ B_y \end{pmatrix} \tag{5}$$

where S_{xy} and S_{yx} are the cross magnetic sensitivities of the sensors. Under ideal conditions, $S_{xx} = S_{yy} = S$ and $S_{xy} = S_{yx} = 0$, the S_{xx} and S_{yy} have a good uniformity. Then, the output voltage (V_{out}) can be denoted by:

$$V_{\text{out}} \sqrt{{V_x}^2 + {V_y}^2} = \sqrt{{S_{xx}}^2 B^2 \cos^2 \theta + {S_{yy}}^2 B^2 \sin^2 \theta} = \boldsymbol{S} \cdot \boldsymbol{B} \quad (6)$$

From Equation (5), we can see that DSI and DSII are used to achieve the measurement of the magnetic field components B_x and B_y in the xy plane, respectively. In addition, the V_{out} of the proposed sensor under the action of $\boldsymbol{B}$ is calculated by Equation (6). When B is a certain value, under the ideal case, the magnetic sensitivity has good uniformity, and V_{out} does not change with θ. After theoretical analysis, the proposed sensor has 2D magnetic sensitive characteristics and can achieve the geographic orientation measurement in plane at the same time.

3. Fabrication Technology

Based on the basic structure of the proposed sensor, the chip of the sensor was fabricated on a double-sided polished p-type <100> orientation silicon wafer with high resistivity. Figure 4 shows the main fabrication process of the sensor. The process steps are as follows: (a) cleaning the silicon wafer by using the Radio Corporation of America (RCA) standard cleaning method; (b) the first oxidation, growing the SiO_2 layer by the thermal oxidation method, with a thickness of 30 nm–40 nm; (c) etching windows of the collector load resistor, injecting phosphorus ions by the ion implantation process and forming collector load resistors; (d) etching windows of the collector region, shaping the n^+ regions adopted phosphorus ion implantation process, photoetching base region windows, concentrated boron injection to form p^+ regions and removing the SiO_2 layer of the upper surface, after re-growth of the SiO_2 layer (thickness of 500 nm); (e) lithography emitter region windows, etching silicon cups by inductively-coupled plasma (ICP) and injecting phosphorus ions to form emitter junctions of four SMSTs; (f) photolithography of the lead hole; the Al layer was deposited on the surface of silicon wafer by the magnetron sputtering method, etching metal Al to form four collectors (C_1, C_2, C_3 and C_4), four bases (B_1, B_2, B_3 and B_4) and the interconnect wire on the surface of the chip, depositing the Al electrode on the back of the wafer to form a common emitter and metallization to form an ohmic contact (30 min at 420 °C).

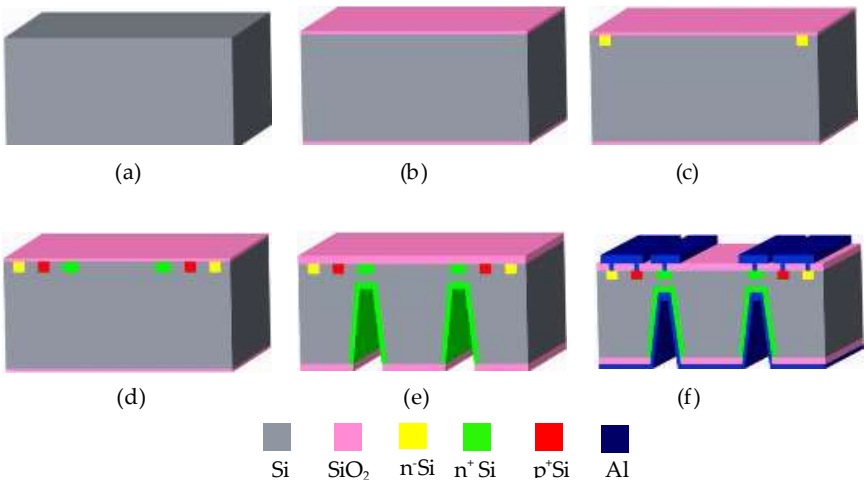

Figure 4. Main fabrication technology process of the proposed sensor chip: (**a**) cleaning the silicon wafer; (**b**) growing thin oxide; (**c**) lithography and ion implantation form load resistors and collector regions; (**d**) making the base regions by lithography and ion implantation; (**e**) lithography and ion implantation to form four emitter regions; (**f**) lithography and deposition of Al electrodes and metallization to form an ohmic contact.

Figure 5a shows the front photograph of the fabricated sensor. The area of the chip is 2.3 mm × 2.3 mm. B_1, B_2, B_3 and B_4 are the bases, C_1, C_2, C_3 and C_4 are the collectors and R_{L1}, R_{L2}, R_{L3} and R_{L4} are the collector load resistors of the four SMSTs. As shown in Figure 5b, E_1, E_2, E_3 and E_4 are the emitters of the four SMSTs, respectively. They form the common emitters. The chip was packaged on printed circuit boards (PCBs) using internal lead bonding technology, and a photograph is shown in Figure 5c.

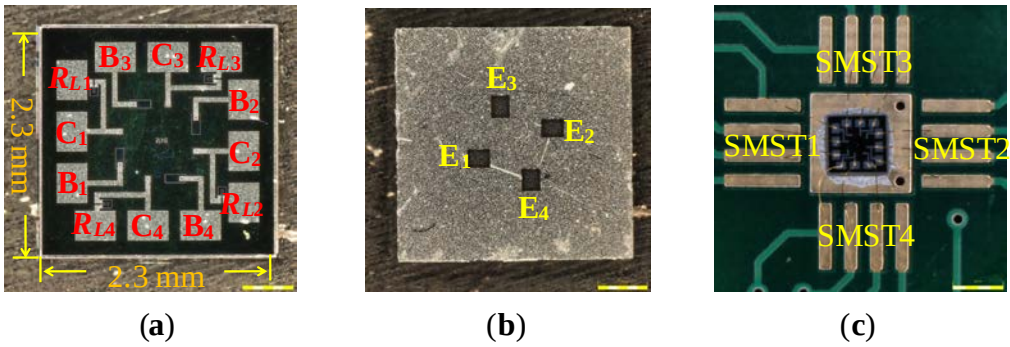

Figure 5. Photograph of the chip of the monolithically-integrated 2D magnetic field sensor: (**a**) front of the chip; (**b**) back of the chip; (**c**) photograph of the packaging of the monolithically-integrated chip.

4. Characteristics of the 2D Magnetic Field Sensor

4.1. Testing System

Figure 6 shows the testing system of the proposed sensor, which consists of a magnetic field generator (CH-100, Cuihai, Beijing, China), a multi-meter (Agilent 34401A, Agilent, Santa Clara, CA, USA), a programmable linear DC power source (DP832A, RIGOL, Beijng, China) and a rotating platform. At room temperature, we studied the I_C-V_{CE} characteristics of the SMSTs using a semiconductor characteristic analysis system (KEITHLEY 4200, Keithley, Cleveland, OH, USA). On this basis, the magnetic sensitive characteristics for the 2D magnetic field sensor were tested using the testing system. In the testing process, the chip of sensor was placed on the surface of a rotating platform. By adopting a rotating platform with a programmable motor, we adjusted the angle (θ) between the constant magnetic field vector ($\boldsymbol{B}$) and the magnetic sensitive direction for the x-axis sensor. According to Equations (1)–(3), when B is constant, the relationship curves between the output voltage (V_x and V_y) and the θ are tested.

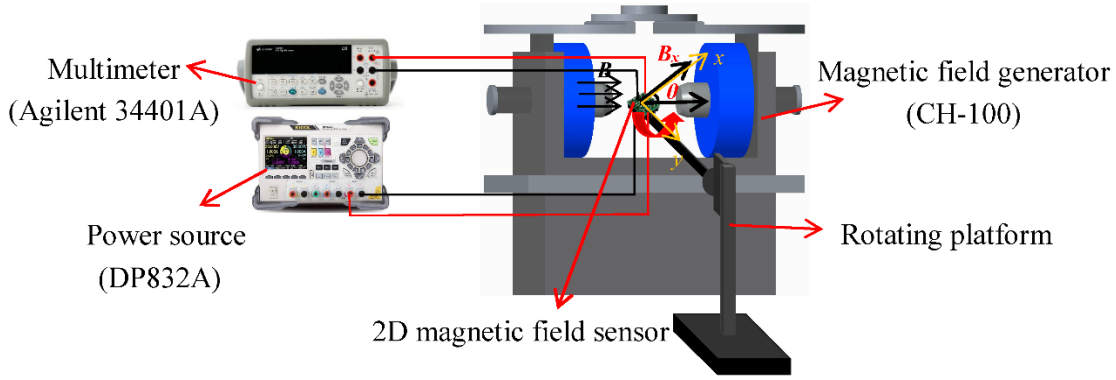

Figure 6. The test system of the monolithically-integrated 2D magnetic field sensor.

4.2. I_C-V_{CE} Characteristics of the SMSTs

In a range of supply collector voltage of 0 V–6.0 V (the test step is 0.2 V) and a base injection current (I_B) of 8.0 mA, the effect of the external magnetic field (B = 0 T, B = ±0.3 T and B = ±0.6 T) on the I_C-V_{CE} characteristics of SMSTs was researched. When a magnetic field is applied on the chip along the x-axis direction, Figure 7a,b shows the I_C-V_{CE} characteristic curves of SMST1 and SMST2 at different B_x (and B_y = 0 T). We can see that SMST1 and SMST2 have the opposite magnetic sensitive characteristics. When V_{CE} > 1.8 V, the I_{C1} of SMST1 keeps increasing in the whole magnetic field range from the positive magnetic field to the negative magnetic field. However, in the same condition, the I_{C2} of SMST2 keeps decreasing. It was also shown that when V_{CE} was a fixed value and B_x > 0 T, the I_{C1} of SMST1 decreased with B_x and the I_{C2} of SMST2 increased with B_x. When B_x < 0 T, the I_{C1} of SMST1 increased with B_x and the I_{C2} of SMST2 decreased with B_x. Furthermore, when a magnetic field B was applied along the y-axis direction (and B_x = 0 T), the I_C-V_{CE} characteristic curves of SMST3 and SMST4 were as shown in Figure 7c,d. Similarly, SMST3 and SMST4 also had the opposite magnetic sensitive characteristics. Moreover, the I_C-V_{CE} characteristic curves of SMST3 and SMST4 were similar to those of SMST1 and SMST2, respectively.

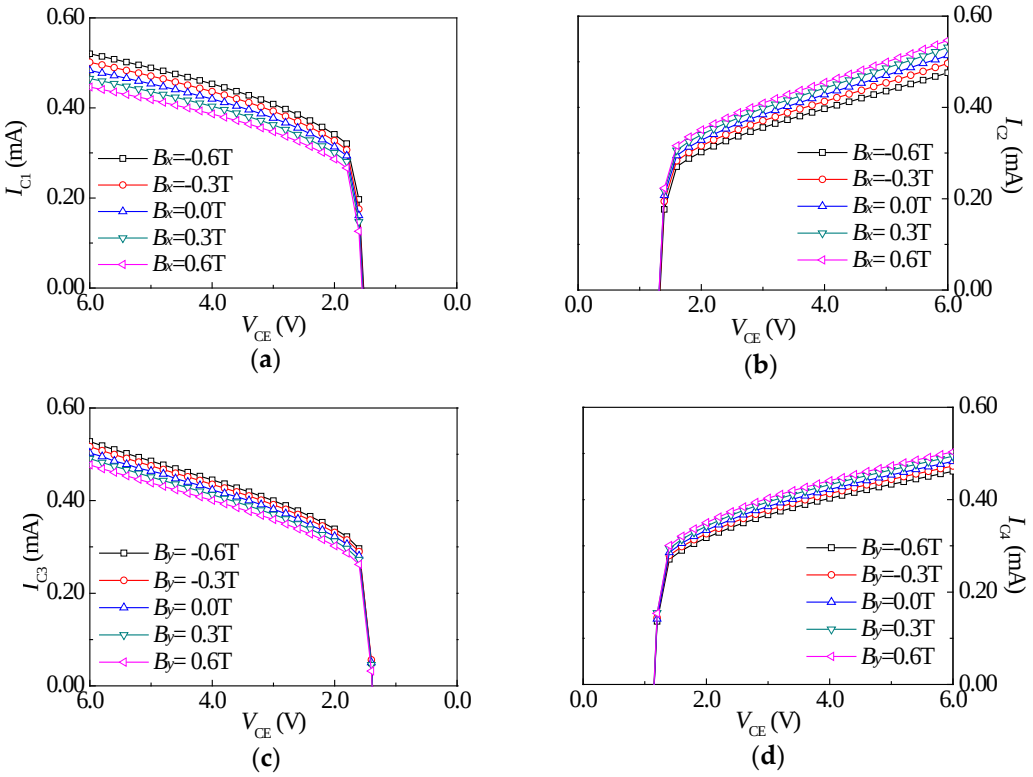

Figure 7. The I_C-V_{CE} characteristic curves of the four SMSTs under different magnetic fields: (**a**) SMST1; (**b**) SMST2; (**c**) SMST3; (**d**) SMST4.

4.3. Magnetic Sensitivity Characteristics

Figure 8 shows the relationship curves between the variation of collector currents for four SMSTs and magnetic field B_x (B_y), where ΔI_{C1}, ΔI_{C2}, ΔI_{C3} and ΔI_{C4} are four collector current variations, respectively. At V_{CE} = 5.0 V, we analyze the effects of I_B on magnetic sensitivity. Figure 8a clearly reveals that when B_x > 0 T (or B_x < 0 T), ΔI_{C1} is less than zero (or greater than zero) and ΔI_{C2} value is greater than zero (or less than zero). When B_x is a fixed value, the absolute value of ΔI_{C1} and ΔI_{C2} increases with I_B. As shown in Figure 8b, under the same conditions, ΔI_{C3} and ΔI_{C4} are similar to

those of ΔI_{C1} and ΔI_{C2}, respectively. The experimental results showed that V_{CE} and B_x (B_y) were fixed values, the absolute value of ΔI_{C1}, ΔI_{C2}, ΔI_{C3} and ΔI_{C4} linearly increasing with I_B.

In light of Figure 2, the input-output characteristics of the SMSTs tested under V_{CE} = 5.0 V and I_B = 8.0 mA are shown in Figure 9. When $B = B_x$, it can be seen from Figure 9a that when $B > 0$ T (or $B < 0$ T), V_{x1} increases with B and V_{x2} decreases with B (or V_{x1} decreases with B and V_{x2} increases with B). The experimental results showed that SMST1 and SMST2 had the opposite magnetic field sensitive directions, while V_{y3} and V_{y4} were almost unchanged, indicating that the magnetic field applied in the direction of the x-axis had little effect on SMST3 and SMST4.

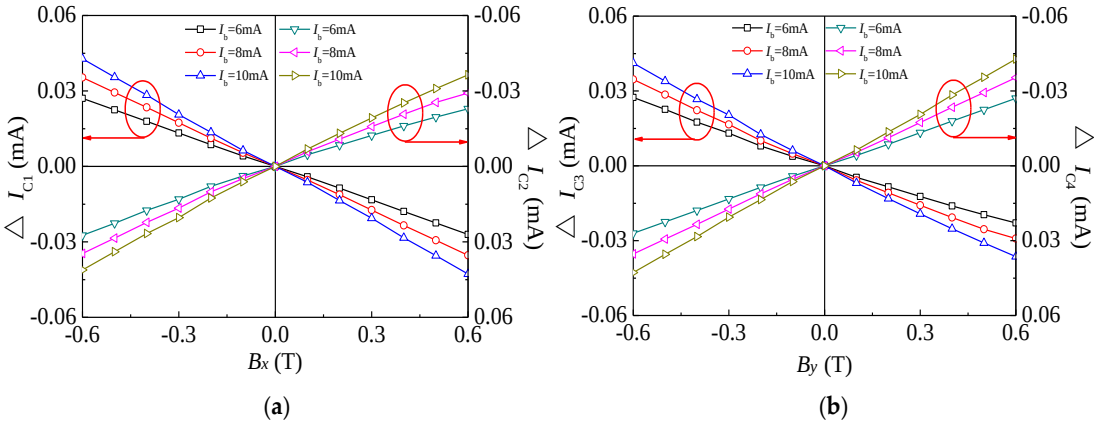

Figure 8. Relationship curves between ΔI_C and B of the four SMSTs: (**a**) SMST1 and SMST2; (**b**) SMST3 and SMST4.

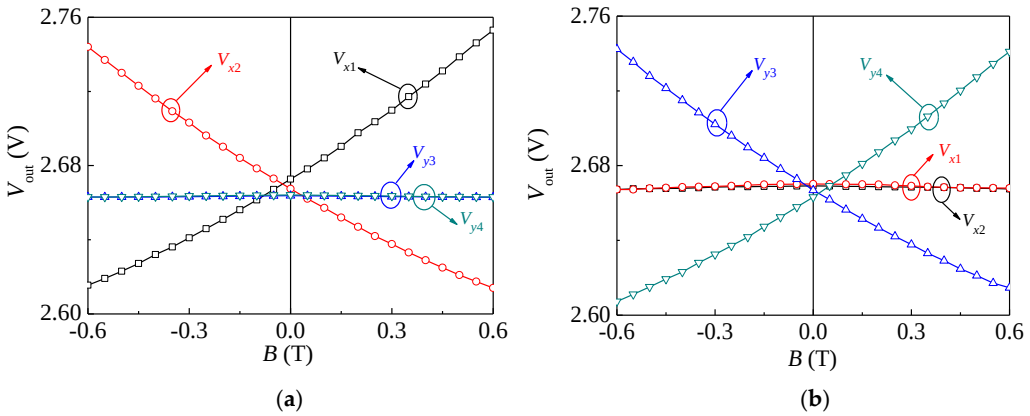

Figure 9. Relationship curves between V_{out} and B of the SMSTs: (**a**) $B = B_x$; (**b**) $B = B_y$.

Moreover, under the same conditions, when the magnetic field was applied along the y-axis direction, the collector output voltage of SMST3 and SMST4 were similar to those of SMST1 and SMST2, respectively. As a result, Figure 9b reveals that when the magnetic field was applied along the y-axis, it only affected SMST3 and SMST4 and had the opposite sensitive direction. In line with Equation (4), the voltage magnetic sensitivities (S_{x1}, S_{x2}, S_{y3} and S_{y4}) of the four SMSTs can be calculated from the experimental results. When V_{CE} = 5.0 V and I_B = 8.0 mA, S_{x1}, S_{x2}, S_{y3} and S_{y4} are 115 mV/T, 108 mV/T, 106 mV/T and 112 mV/T, respectively.

The relationship curves between V_x (V_y) of the x-axis and y-axis sensors and B are shown in Figure 10, which shows that V_x and V_y had better linearity with changing B, and the proposed sensor could detect the 2D magnetic field. As obtained from Equation (4), S_{xx} and S_{yy} of DSI and DSII were 223 mV/T and 218 mV/T, respectively. Based on Equation (5), S_{xy} and S_{yx} of DSI and DSII were 0.43 mV/T and 0.08 mV/T, respectively. On the basis of the definition of cross interference [13],

the cross interference was found to be 0.19% and 0.04%, respectively. The results showed that the sensitivities of the sensor could be improved with better uniformity and lower cross interference.

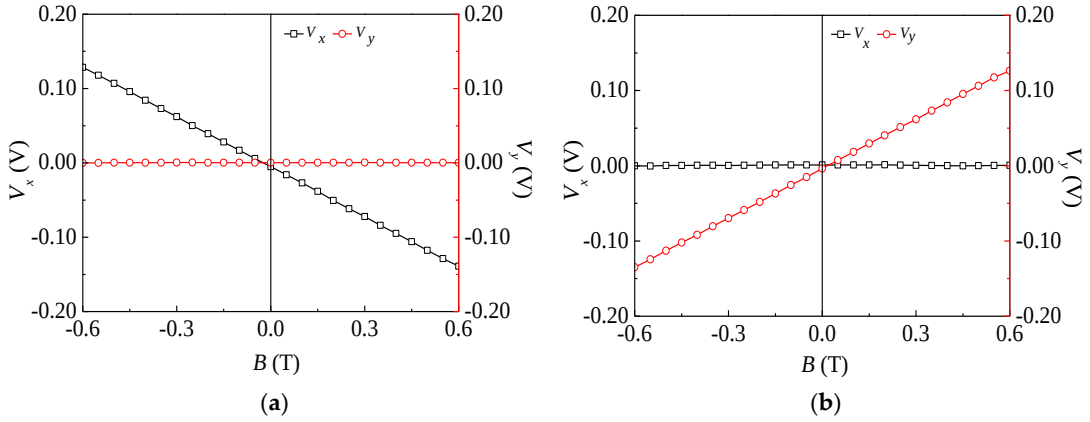

Figure 10. Relationship curves of V_x~B, V_y~B of the 2D magnetic field sensor: (**a**) $B = B_x$; (**b**) $B = B_y$.

4.4. Characteristics of the 2D Magnetic Field Sensor

When V_{DD} = 5.0 V and I_B = 8.0 mA, Figure 11a,b shows the relationship curves between V_x (V_y) and rotation angle θ (from 0° to 360° with a step of 5°). Under the condition of B = 0.4 T, we rotated the chip, when θ = 0° ($B = B_x$ and B_y = 0 T), V_x was maximum and V_y was approximately zero. With the increasing of θ, V_y increased and V_x decreased. When θ = 45°, in theory, $B_x = B_y = \sqrt{2}B/2$, the experimental results showed that V_x = 53.1 mV and V_y = 58.9 mV. When θ = 90°, the experimental results showed that $V_x = -6.5$ mV and V_y = 80.1 mV. From Figure 11a, we can see that V_x and V_y varied with θ and conformed to the sine and cosine functional relationship. Through the analysis of the experimental results, the proposed sensor could detect B_x and B_y in the xy plane, respectively. According to Equation (6), we calculated the V_{out} of the sensor at different rotation angles. Figure 11b shows the relationship curves between V_{out} and θ, and V_{out} was close to the circular. The results showed that the magnetic sensitivities along the x-axis and y-axis direction of the 2D magnetic field sensor approached uniformity.

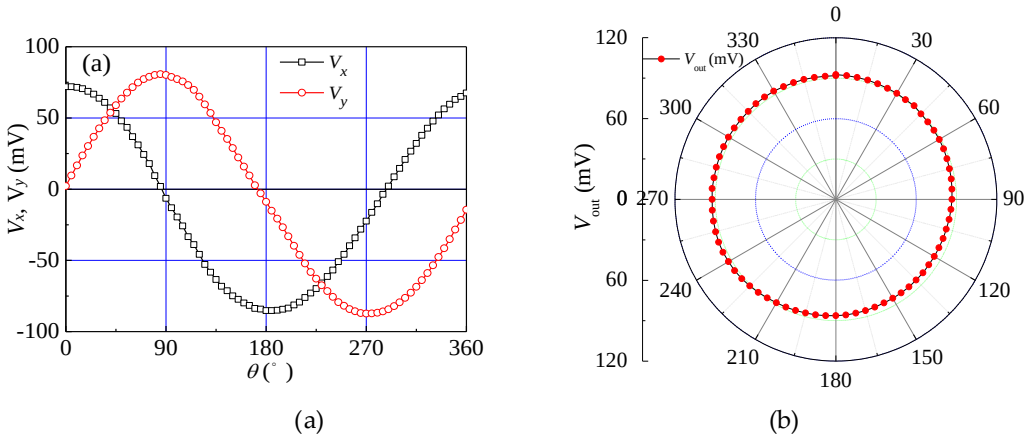

Figure 11. Relationship curves between the output voltage and rotation angle θ of the proposed sensor: (**a**) V_x~θ and V_y~θ; (**b**) V_{out}~θ.

Table 1 gives a summary of the performance of the 2D magnetic field sensors [9–12]. In this work, the monolithically-integrated magnetic field sensor based on four SMSTs and four collector load resistors had higher magnetic sensitivity and lower cross interference.

Table 1. Performance summary and comparison of 2D magnetic field sensors.

Reference Parameters	Magnetic Sensitive Structure	Supply Voltage	Magnetic Sensitivity	Cross Interference	Chip Area
[9]	Hall device	2.7 V	9.56 mV/T	0.259 mV (B = 150 mT) 0.330 mV (B = 150 mT)	2.0 × 1.0 mm^2
[10]	Vertical Hall device	—	S_x = 40.06 mV/(V·T) S_y = 42.65 mV/(V·T)	12.55 mV/(V·T) 12.33 mV/(V·T)	—
[11]	Hall device	5.0 V	34.0 mV/(V·T)	—	60.0 × 60.0 μm^2
[12]	Magnetic sensitive transistor	V_{CE} = 10.0 V I_B = 6.0 mA	S_x = 366 mV/T S_y = 365 mV/T	—	7.0 × 7.0 mm^2
This work	Magnetic sensitive transistor	V_{CE} = 5.0 V I_B = 8.0 mA	S_x = 223 mV/T S_y = 218 mV/T	0.19% 0.04%	2.3 × 2.3 mm^2

5. Conclusions

In summary, a monolithically-integrated 2D magnetic field sensor was designed and fabricated on a silicon wafer with the <100> direction (ρ > 100 Ω·cm) using MEMS technology and packaged on PCBs. It consisted of two difference structures with four SMSTs and four collector load resistors. When V_{CE} = 5.0 V and I_B = 8.0 mA, the magnetic sensitivities of the two difference structures for the proposed sensor were 223 mV/T and 218 mV/T, respectively. The S_{xx} and S_{yy} were approximately equal, indicating that the magnetic sensitivity of the proposed sensor had better uniformity. Through the characteristics analysis of the proposed sensor, the relationship curves between output voltage (V_x, V_y) and θ conformed to the sine function and cosine function at a constant external magnetic field (B), so the proposed sensor could detect the magnetic field vector $\boldsymbol{B}$ in the xy plane and exhibited lower cross interference, which lays the foundation for the research on the measurement of a 2D magnetic field and for the monolithic integration of the sensor.

Author Contributions: Supervision, X.Z. and D.W.; Validation, C.J., M.L.; Visualization, Q.D.; Writing, original draft, X.Z., C.J. and Q.D.; Writing, review and editing, X.Z.

Funding: Project supported by the National Natural Science Foundation of China (Grant Nos. 61471159, 61006057), the Special Funds for Science and Technology Innovation Talents of Harbin in China under Grant 2016RAXXJ016 and the Modern Sensor Technology Innovation Team for the College of Heilongjiang Province in China (Grant No. 2012TD007).

Conflicts of Interest: The authors declare no conflict of interest.

References

1. Roumenin, C.S.; Nikolov, D.; Ivanov, A. A novel parallel-field Hall sensor with low offset and temperature drift based 2D integrated magnetometer. *Sens. Actuators A Phys.* **2004**, *115*, 303–307. [CrossRef]
2. Herrera-May, A.L.; Soler-Balcazar, J.C.; Vázquez-Leal, H.; Martínez-Castillo, J.; Vigueras-Zuñiga, M.O.; Aguilera-Cortés, L.A. Recent advances of MEMS resonators for lorentz force based magnetic field sensors: Design, Applications and Challenges. *Sensors* **2016**, *16*, 1359. [CrossRef] [PubMed]
3. Zhao, X.F.; Li, B.Z.; Wen, D.Z. Fabrication technology and characteristics of a magnetic sensitive transistor with nc-Si:H/c-Si heterojunction. *Sensors* **2017**, *17*, 212. [CrossRef] [PubMed]
4. Sander, C.; Leube, C.; Paul, O. Novel compact two-dimensional CMOS vertical Hall sensor. In Proceedings of the 2015 Transducers—2015 18th International Conference on Solid-State Sensors, Actuators and Microsystems (TRANSDUCERS), Anchorage, AK, USA, 21–25 June 2015; pp. 1164–1167.
5. Roumenin, C.S. Magnetic sensors continue to advance towards perfection. *Sens. Actuators A Phys.* **1995**, *46-47*, 273–279. [CrossRef]
6. DJiles, C.; Lo, C.C.H. The role of new materials in the development of magnetic sensors and actuators. *Sens. Actuators A Phys.* **2003**, *106*, 3–7.

7. Banjevic, M.; Furrer, B.; Popovic, R.S. 2D CMOS integrated magnetometer based on the miniaturized circular vertical Hall device. In Proceedings of the 2009 International Solid-State Sensors, Actuators and Microsystems Conference, Denver, CO, USA, 21–25 June 2009; pp. 877–880.
8. Zhao, X.F.; Wen, D.Z.; Zhuang, C.C.; Cao, J.; Wang, Z. Fabrication and characteristics of the magnetic field sensors based on nano-polysilicon thin-film transistors. *J. Semicond.* **2013**, *34*, 036001. [CrossRef]
9. Yu, C.P.; Sung, G.M. Two-dimensional folded CMOS Hall device with interacting lateral magnetotransistor and magnetoresistor. *Sens. Actuators A Phys.* **2012**, *182*, 6–15. [CrossRef]
10. Sung, G.M.; Yu, C.P. 2-D differential folded vertical Hall device fabricated on a P-Type substrate using CMOS technology. *IEEE Sens. J.* **2013**, *13*, 2253–2262. [CrossRef]
11. Huang, H.Y.; Wang, D.J.; Xu, Y. A monolithic CMOS magnetic Hall sensor with high sensitivity and linearity characteristics. *Sensors* **2015**, *15*, 27359–27373. [CrossRef] [PubMed]
12. Yang, X.H.; Zhao, X.F.; Bai, Y.J.; Wen, D. Two-Dimensional magnetic field sensor based on silicon magnetic sensitive transistors with differential structure. *Micromachines* **2017**, *8*, 95. [CrossRef]
13. Lozanova, S.; Noykov, S.; Roumenin, C. Three-dimensional magnetometer based on subsequent measurement principle. *Sens. Actuators A Phys.* **2015**, *222*, 329–334. [CrossRef]